



Landslide susceptibility mapping of the Tehri reservoir rim area using the weights of evidence method

ROHAN KUMAR^{1,*} and R ANBALAGAN²

¹*Punjab Engineering College (Deemed-to-be University), Vidya Path, Sector 12, Chandigarh 160 012, India.*

²*Department of Earth Sciences, Indian Institute of Technology Roorkee, Roorkee 247 667, India.*

*Corresponding author. e-mail: rohananadi@yahoo.com

MS received 30 January 2018; revised 2 January 2019; accepted 4 January 2019; published online 4 June 2019

This study was aimed to utilise important landslide causal factors for the delineation of the landslide susceptible area using the weights of evidence (WofE) method in the Tehri reservoir rim region on a macro scale. The Tehri reservoir extends up to 70 km and bounded by moderate to steep slopes. Landslide susceptibility mapping (LSM) is an essential measure for identifying the potentially unstable slopes bounding the reservoir. With the help of ancillary data, remote sensing imagery and a digital elevation model, 10 causative factors along with landslide inventory were extracted. Initially, the WofE model was applied to obtain the association between landslides and causative factors. The process gave the numerical estimate of correlation between landslides and causative factors by means of positive and negative correlation. Important factor attributes, potentially causing landslides, were identified based on high positive correlation values. Later, the posterior probability of landslide occurrence for each mapping unit was also computed using the WofE model. Posterior probability was divided into five relative susceptibility classes. Validation of the posterior probability map was carried out by using the prediction rate curve technique and a reasonable accuracy of 83% was achieved. LSM of the Tehri reservoir rim area implicates unplanned road construction and settlements coupled with the reservoir slope settlement process for the present degradation of the geo-environmental system in that region.

Keywords. Landslide; susceptibility; Tehri; reservoir rim; weights of evidence; GIS.

1. Introduction

Natural disasters have become a very common phenomenon all over the world. Significant amount of planning and mitigation works are being carried out to tackle the risks associated with the disaster events. Devastation following the natural hazards is often associated with anthropogenic interference in the geo-environment. Some eye-opening instances of such recent phenomena are the 2011 Japan tsunami (Fritz *et al.* 2011) and the 2013 Kedarnath floods, Uttarakhand, India (Dobhal *et al.* 2013). Various types of natural

hazards such as typhoon, tsunami, flash flood, hurricane, earthquake, slope subsidence, etc., have become major threats to all living creatures. Hilly terrains are susceptible to multiple hazards such as earthquakes, avalanches, cloud bursts, etc., but landslides are dominant. Disaster studies on a global scale have emphasised that developing countries such as India, China and Nepal have suffered high destruction and fatalities due to the landslide hazard in the past decade (OFDA/CRED 2010). Estimates suggest that out of 80% landslide-related fatalities reported from developing countries, India accounts for 8% of them

(Kirschbaum *et al.* 2010). About 15% of the total land coverage of India is susceptible to landslides (NDMA 2009; Kundu *et al.* 2013). Triggering factors, namely, earthquakes, excessive rainfall and intense anthropogenic activity are the main reasons for landslides in India.

Landslide hazard and risk evaluation can be achieved by supplying risk managers with easily available, continuous and precise knowledge about landslide susceptibility (Kouli *et al.* 2013). By means of scientific investigation, we can evaluate and forecast landslide prone regions, and thus minimise landslide destruction by implementing suitable mitigation measures (Saha *et al.* 2005; Pradhan 2010; Kundu *et al.* 2013).

Landslide susceptibility mapping (LSM) is a component of preparedness measure against probable landslide hazard event. LSM gives the knowledge of landslide propensity in advance on account of existing ground physical conditions. The identification of the landslide susceptible area is rooted in the premise that future landslides are expected under the geo-environmental settings which have been responsible for landslides in the present and in the past (Varnes 1984; Pardeshi *et al.* 2013; Kumar and Anbalagan 2015). The reliability of LSM is governed by the choice of landslide causative factors, distribution of factors in the given area and applicable methodology. Many techniques are exercised for the identification of landslide susceptible regions. They are generally categorised in qualitative, semi-quantitative, quantitative/probabilistic, deterministic/analytical and process-based methods. Qualitative methods are based on assigning propensity values to the factors by expert knowledge and hence they are very subjective in nature. For the regional susceptibility analysis, qualitative methods have been proven useful (Anbalagan 1992; Gupta and Anbalagan 1997; Gupta *et al.* 2008). Examples of semi-quantitative techniques are weighted linear combination, fuzzy logic and analytic hierarchy process. These logical tools are subjected to quantify the significance of landslide causative factors in terms of weights/ratings (Guzzetti *et al.* 1999; Akgun *et al.* 2008; Pourghasemi *et al.* 2012; Yan *et al.* 2019). The foundation of probabilistic methods lies in landslide density within factor classes. Bivariate and multivariate statistics are the two variants of the probabilistic–statistical method. Bivariate statistical models are based on the correlation between landslide distribution and landslide factors. These models compute weights/ratings

of each factor class. Weights of evidence (WofE), frequency ratio, information value, a combination of frequency ratio and fuzzy logic are important bivariate statistical methods which are practiced in the landslide susceptibility study (Mathew *et al.* 2007; Akgun *et al.* 2008; Kannan *et al.* 2013; Sujatha *et al.* 2014; Sharma and Mahajan 2018). Multivariate models are also based on landslide density but in order to compute the landslide probability, they use the collective influence of factors (Das *et al.* 2012; Umar *et al.* 2014; Shahabi *et al.* 2015; Kalantar *et al.* 2018). A commonly practiced multivariate statistical method is the logistic regression method (Nandi and Shakoor 2009). Another common method for determining slope failure susceptibility is the analytical/deterministic method, which uses geotechnical features such as slope morphometry, structural discontinuity pattern, soil moisture, etc., to estimate the susceptibility by means of a factor of safety (Chakraborty and Anbalagan 2008; Akgun and Erkan 2016; Sarkar *et al.* 2016; Ciarleo *et al.* 2017). Nowadays, deep machine learning algorithms such as decision trees, fuzzy neural networks, support vector machines and adaptive neuro-fuzzy interface system models (Arora *et al.* 2004; Kanungo *et al.* 2006; Yao *et al.* 2008; Yilmaz 2010; Kumar *et al.* 2017; Hong *et al.* 2018) are extensively used for identifying landslide susceptible zones.

In the present work, a bivariate statistical method, ‘WofE’, was attempted to carry out the susceptibility study. The foundation of WofE lies in Bayesian statistics, and uses the prior probability of occurrence of an event such as landslide to compute its posterior probability on the basis of the correlation between the evidential themes and landslide inventory. In this work, we aimed for the applicability of the WofE method in identifying the landslide propensity of the Tehri reservoir rim area. Several authors have successfully attempted the WofE model in different parts of the Himalaya to obtain a degree of the susceptibility of terrain (Mathew *et al.* 2007; Dahal *et al.* 2008; Ghosh *et al.* 2009; Kayastha *et al.* 2012). In most of the above-mentioned techniques, the ratings of factor classes were obtained on the basis of the WofE, formulations and rated thematic layers were arithmetically overlaid to determine the degree of susceptibility. In this work, the posterior probability of landslide occurrence was identified considering existing landslide inventory and factor classes together. Given the extent of the slopes bounding the reservoir, this work was carried out on a macro scale of 1:50,000.

2. Study area

The Tehri reservoir rim area is located in the highly undulating terrain of the Lesser Himalaya (figure 1). Here, the reservoir rim area refers to the area bounding the reservoir. The Tehri reservoir has developed partly in the Bhagirathi and partly in the Bhilangana rivers as a result of the construction of the Tehri dam and it extends in length up to 70 km. The reservoir is bounded by moderate to steep slopes which support settlements, forest land, crop land, etc. This area is represented by cliffs, ridges, spurs, deeply dissected valleys, well-developed terraces and abrupt sharp slopes. Ridges and spurs are occupied by dense to sparse forests. Moderate slopes are generally supported by agricultural lands, plantation and settlements. The area is drained by a typical mountainous drainage pattern such as parallel, sub-parallel and sub-dendrite patterns.

A number of development works are in the construction or completion phase on the slopes bounding the Tehri reservoir. This huge reservoir is filled during the monsoon season and dries out substantially in the summer season. Additionally, during the reservoir operation, some degree of drawdown occurs. The reservoir drawdown takes place between the maximum reservoir level (MRL 830 m) and dead storage level (740 m) during the rainy and summer seasons.

When the reservoir attains MRL, it soaks bounding slopes. The saturated slopes fail at a number of places at the time of sudden drawdown. Instability in the bounding slopes depends upon the following factors: (i) nature of slope forming material, (ii) slope geometry, (iii) vegetation support on slopes and (iv) anthropogenic activity along the reservoir. Reservoir water fluctuation leads to the instability of slopes and these are manifested in terms of landslides, subsidence, sink holes, etc. Typical arcuate shape landslides (also called reservoir-induced landslides) which originate at the reservoir level have been found progressing towards the upper reaches of slopes and encroaching settlements. Additionally, roads have been constructed by randomly cutting the reservoir bounding slopes and this has only aggravated the instability problem in the reservoir rim area.

2.1 Geology of the Tehri reservoir region

The most significant geological investigation of Tehri area was pioneered by Valdiya (1980). The

reservoir region belongs to the great Himalayan division called the Lesser Himalaya. Henceforth, rocks in the Tehri reservoir area are represented by various litho units of the Lesser Himalaya. Rautgara, Chandpur, Nagthat, Deoban, Krol and Blaini formations of Damtha, Jaunsar, Tejam and Mussoorie groups, respectively, are the major rock units occupying the area. Table 1 illustrates the stratigraphic succession of Tehri area. Extremely worn quartzite and phyllite (moderate to low grade) of Chandpur formation are characteristic of the central part of the reservoir rim region. Characteristic structural discontinuities such as foliation plane and joints make phyllite and quartzite vulnerable to landslides. In the western segment of the study area, Nagthat quartzites are dominantly present. These quartzites are characterised by different colours and often found intercalated with slates. Due to the frequent presence of weathered top and shearing, Nagthat rocks are vulnerable to landslides at places. In the eastern segment, the North Almora thrust (NAT) divides the Jaunsar group from the Damtha group. Rocks affiliated to the Rautgara formation consist of varying colours of quartzite (dominant), slates (minor presence) and metavolcanics. Rocks affiliated to Deoban formation are seen in the eastern portion of the area. Deoban formation is stuffed between the Berinag and Rautgara formation in the southern segment of the area. It consists of fine-grained dolomitic limestone with minor phyllitic intercalations. Rocks of the Deoban formation are largely represented at the higher ridges. Rocks affiliated to the Berinag formation are manifested in the eastern segment of the region. The Berinag thrust disconnects this formation from its base.

Rocks associated with the Berinag formation are mainly quartzite. Quartzite slates and carbonate rocks affiliated to the Blaini formation are represented in the western portion of the study area. The area is also represented by three regional structures including two syncline zones and a thrust fault 'NAT' (figure 2).

The area is represented by a variety of structural discontinuities such as foliation plane, bedding plane, joints, faults and shear zone. But the most important discontinuities observed on the slope faces are the foliation planes, joint set and shear zone. Rocks found adjacent to the reservoir are mainly phyllite. General orientation of the foliation plane is of three types: 45–55°/N170–180, 40–45°/N200–210 and 40–50°/N120–130. These planes generally dip into the hill, except at places where it

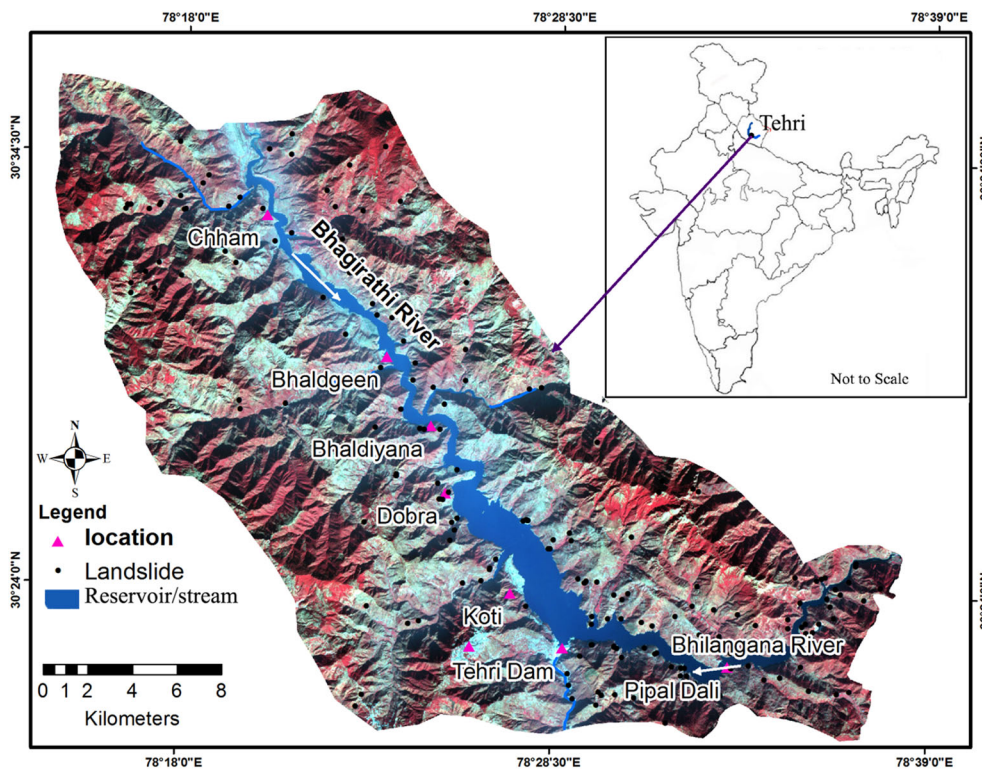


Figure 1. Study area: the Tehri reservoir rim region.

Table 1. Illustration of stratigraphic classes present in the Tehri region.

Age	Group	Formations and rock type
Cambrian	Mussoorie	Krol formation: Outer Lesser Himalaya Rock type: limestone intercalated with slates and siltstone
Neoproterozoic	Mussoorie	Blaini formation: Outer Lesser Himalaya Rock type: quartzite, limestone, slates, phyllites and conglomerate
Mesoproterozoic	Jaunsar	Berinag formation: Inner Lesser Himalaya Rock type: weathered quartzite intercalated with slate
		Nagthat formation: Outer Lesser Himalaya Rock type: weathered quartzite intercalated with slate
	Jaunsar	Chandpur formation: Outer Lesser Himalaya Rock type: low grade lustrous phyllites
Mesoproterozoic	Tejam	Deoban formation: Inner Lesser Himalaya Rock type: dolomitic limestone with phyllitic intercalations
		Mandhali formation: Outer Lesser Himalaya Rock type: dolomitic limestone with phyllitic intercalations
		Rautgara formation: Inner Lesser Himalaya Rock type: quartzite, slate, metavolcanic rocks
Mesoproterozoic (>1300 myr)	Damtha	

dips parallel to the stream. Three dominant joint sets have been observed in the slopes. The first set of joints is the bedding joint featured by a

longer extent (130–175°/50–90°), the second set of joints is the cleavage joint (50–100°/30–50°) and the third set of joints is the linear zones of

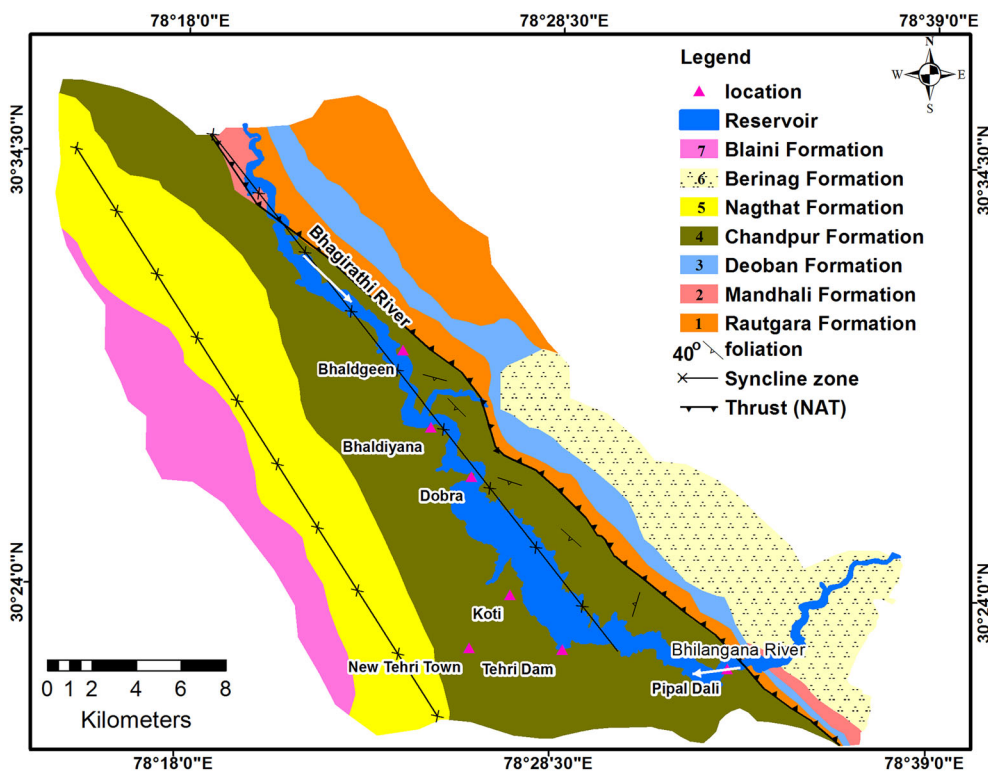


Figure 2. Geological map of the Tehri region (after Valdiya 1980).

intensive jointing ($210\text{--}270^\circ/30\text{--}60^\circ$). A large number of shear zones of varying dimensions were also observed.

2.2 Landslide inventory of the area

A total of 195 landslides were mapped through field observations, image interpretation and historical information. Out of the total, 18% of the landslides were mapped on a macro scale and the rest were micro landslides. The general dimension of the landslides was found in the range of $50\text{--}3000\text{ m}^2$. A large number of slope failure phenomena were observed on the lower level of slopes bounding the Tehri reservoir. These make distinctive arcuate shapes and also called reservoir-induced landslides (figure 3a). Such landslides were found to be occurring predominantly on the talus slopes due to reservoir drawdown. Reservoir water-level variation also leads to failure in river terraces, which are composed of alluvial material (figure 3b). The advancing characteristic of reservoir-induced landslides has turned out to be major risk to the inhabitants of the higher slopes also. Many landslides were seen alongside the roads constructed on the reservoir-bounding slopes. In the recent

past, the density of road network on these slopes has increased substantially. These roads were constructed by cutting the slopes randomly and leaving the scarp face untreated. All through the rainy season, the untreated cut slopes fail at number of places. Such failures were observed in the debris/river-borne material (RBM) slopes as well as in rocky slopes (figure 3c and d). Characteristic translational failures were observed in slopes, which are composed of phyllite and quartzite rocks (figure 3e).

The study area belongs to the highly undulating Lesser Himalayan terrain comprising a variety of lineaments of different dimensions. Linear structural discontinuities can be captured in the high resolution satellite images and these captured ones are called photo-lineaments (Gupta 2018). Many landslides were seen linked with photo-lineaments, namely, ridges, joints, thrusts, spurs, etc. Very complex and extremely dissected streams drain this area. In the rainy season, these streams erode their banks briskly owing to high stream power. Regardless of the slope-forming material, the eroded portion of the stream bank develops into a spot of continuous landslide (figure 3f). Many landslides were also seen in the settlement/build-up areas and barren slopes.



Figure 3. Field photographs: (a) typical arcuate shape scar of the reservoir-induced landslide, (b) slope failure in RBM, (c) rotational failure along the road network, (d) rotational failure in debris along the road and (e) slope form of phyllite is subjected to plain failure and (f) drainage-induced landslide.

The landslides observed in the study area can be grouped into plane failure, rotational failure and Talus slope failure categories. Rotational failures, which account for $>80\%$ of the total landslide are found along the ridges, roads and lower elevation slopes bounding the reservoir. At a number of places, the reservoir bounding slopes are seen in distress due to Talus failure. In the case of Talus failure, shallow debris or soil material, overlying the base rock, fail along the slope direction. Plane or translational failures are mainly seen in phyllite

and quartzite rocks and they take place along the plane of weakness such as foliation planes, joint planes, etc.

3. Data preparation

Ten landslide causing factors were selected for analysing the susceptibility of the area. Remote-sensing imageries, which are used for the extraction of geo-environmental factors, are listed in table 2.

Table 2. *Details of the data set.*

Data type	Sensor	Resolution/ scale	Data derivative	Data source
Multispectral data	ASTER	15 m	LULC	NASA Reverb
	Landsat series	30 m	Photo-lineament	USGS
	IRS-LISS III	23.5 m	Landslide inventory	NRSC
	World view-2	0.5 m (PAN)		Digital globe
DEM	ASTER GDEM	30 m	Slope Aspect Relative relief Drainage	NASA Reverb
Ancillary data	Published geology map	1:250,000	Digitised geology map	Himalayan Geology Journal
	Published report on soils of Uttarakhand	1:250,000	Digitised soil map	Watershed Management Directorate, Dehradun
	Survey of India Toposheet 53 J/7 NW	1:25,000	Digitised base map	Survey of India

ENVI 4.5 software was employed for the processing of Advanced Spaceborne Thermal Emission and Reflection Radiometer (ASTER) multispectral data. Processing was carried out for geo-referencing the image according to Universal Transverse Mercator (UTM) grids and extraction of visible and near infrared (VNIR) band. World view-2 panchromatic data was obtained in the corrected form, requiring UTM grid coordinates. Landsat 7 data of pre-2003 yr were also acquired in the corrected form. Using the nearest neighbourhood re-sampling method, ASTER VNIR, ASTER global digital elevation model (GDEM) and Landsat 7 VNIR data were re-sampled to 25 m × 25 m pixel size. ASTER DEM was taken through DEM augmentation procedures, for instance, DEM fill/sink elimination for additional study. A panchromatic image of World view-2 sensor having a 50-cm spatial resolution was visually interrelated for extracting the landslide inventory. Digital image processing methods, namely, normalised difference vegetation index (NDVI), supervised classification and band ratio were exercised for retrieving landslide information, land use land cover (LULC) and photo-lineament from the satellite imageries. Additionally, onscreen visualisation techniques were also exercised for the detection of LULC distribution, landslide distribution and photo-lineaments. In addition to satellite imageries, ancillary data, namely, topographic sheet, historical landslide data, soil exposure map and geological map were obtained from various sources. As per the cell size (25 m × 25 m) chosen for LSM, ancillary data were converted into the raster format. Co-registration of satellite imageries

and ancillary data was performed and a precision of half per pixel was achieved. A base map was generated using multisource data and as per the base map, 10 landslide causative factors were extracted in the raster form.

3.1 *Lithology*

Lithology is an important causative factor for the instability of the terrain. A lithology map of the area was prepared showing the distribution of various rock types belonging to different formations. During the field investigation, different rock types and their weathering status have been studied. The contact between different rocks units have been observed in order to prepare a lithology map. The dominant rock type in the study area was of phyllites and quartzites. Other important lithological units are quartzite with minor bands of phyllite, phyllite with minor bands of quartzite, limestone with minor bands of quartzite and slate, lime stone with alternating bands of quartzite and phyllite, quartzite with minor bands of slates and phyllites, slate with minor bands of quartzites, river-borne materials, phyllites with minor bands of limestone, conglomerate and quartzite and slates. The distribution of these rocks is shown in figure 2.

Phyllite covers the major part of the study area and is exposed on both the banks of the Bhagirathi and Bhilangana rivers along with other major tributaries. These rocks are generally vulnerable and are present in the valley region. In general, near the confluence of the Bhagirathi

and Bhilangana rivers, exposed rocks are relatively hard, compact and siliceous in nature. The other most dominant rock of the area is quartzite. It is generally hard and compact and can be found in the higher reaches of the region. Quartzites with minor bands of phyllite are weak in comparison with quartzites. These rocks are mainly exposed in the central part of the region. Phyllite with minor bands of quartzite is mainly occupied in the northern region. These rocks are on both sides of the Bhagirathi river in the south-eastern corner of the area. Limestones with minor bands of quartzite and slate, exposed in the south-western region are bedded and hard in nature. Limestone exposed in the western region of the area is generally hard in nature. Alternate bands of quartzite and phyllite are encountered in the south-western region along the right bank of the Maniyar river, a tributary of the Bhagirathi river. The thickness of the phyllite and quartzite bands is more or less equal. Slates with minor bands of quartzite are exposed in the southern region. The quartzites with minor bands of slate and phyllite are exposed in the southern region along the right bank of the Hunal river. River-borne materials are present at the lower levels on both the banks of the Bhagirathi river. These older terrace materials form a fertile agricultural land. Phyllite with minor bands of limestone, conglomerate and quartzite are also seen to the south of the Chamba town. Slate, which contributes to less than one per cent of the study area, is exposed in the western region.

3.2 Soil cover

The area is represented by the following three categories of soil types: black/forest clay soil, alluvial/sandy loam and sandy loam (figure 4a). Soil type of the area varies with the relief/elevation and annual rainfall. Elevation in the present area varies roughly from 500 to 2600 m, whereas rainfall variation depends on the topographic aspect of slopes (WMDD 2009). Lower level slopes (600–1000 m) are occupied by a mixture of alluvial soil with boulders of varying dimensions. In the middle elevation level (1000–1500 m), soils are mainly the sandy loam type. Black soil and forest soils are present at the higher elevations (>1500 m). Soil categories of the area influence the landslide susceptibility condition. Forest and black clay soils are comparatively less liable to slope failures because of thick vegetation support. Recent alluvium and

loose boulders are more prone to mass movement owing to less compaction and high moisture. Old alluvial deposits seen as terraces in different levels adjoining the river courses on either side particularly on the left side are more stable because of high compaction and high friction. Sandy loamy soil is also weather-prone due to less cementation and compaction. Several cones of debris which were formed because of older landslides consist of assorted sizes of material, ranging from clay to boulder size. They are seen at a number of places, mainly adjoining the river course due to past landslides.

3.3 Land use land cover

LULC design of the area plays a vital role in the landslide hazard study. Amalgamation of the remote sensing image and the topographic map resulted in the following five classes of LULC: (i) dense forest, (ii) scrub forest, (iii) agricultural land, (iv) settlement/barren land and (v) water body (figure 4b). A multispectral VNIR image of the ASTER sensor was subjected to supervised classification and NDVI analysis for the extraction of LULC classes. Vegetation categories were obtained using NDVI thresholds and other LULC categories from supervised classification. LULC classes were extracted with 78% of accuracy. Most of the landslide incidences were found to be associated with settlement/barren land class and agricultural land class.

3.4 Slope angle

ASTER DEM was used to derive the continuous slope angle information. Slope angle was found to be varying in the range of 0–70°, and it was categorised into the following five relative classes: very low (0–8°), low (8–18°), moderate (18–30°), high (30–42°) and very high (>42°) according to its inherent influence on the landslide (figure 4c). In the absence of universally accepted criteria of slope angle classification, the distribution of existing landslides under different ranges of slope angles was considered to classify continuous slope angle data into relative classes. It is commonly perceived that the regions of high slope gradient are more susceptible to landslides compared to regions having a low slope gradient (Anbalagan 1992; Saha *et al.* 2005; Anbalagan *et al.* 2015).

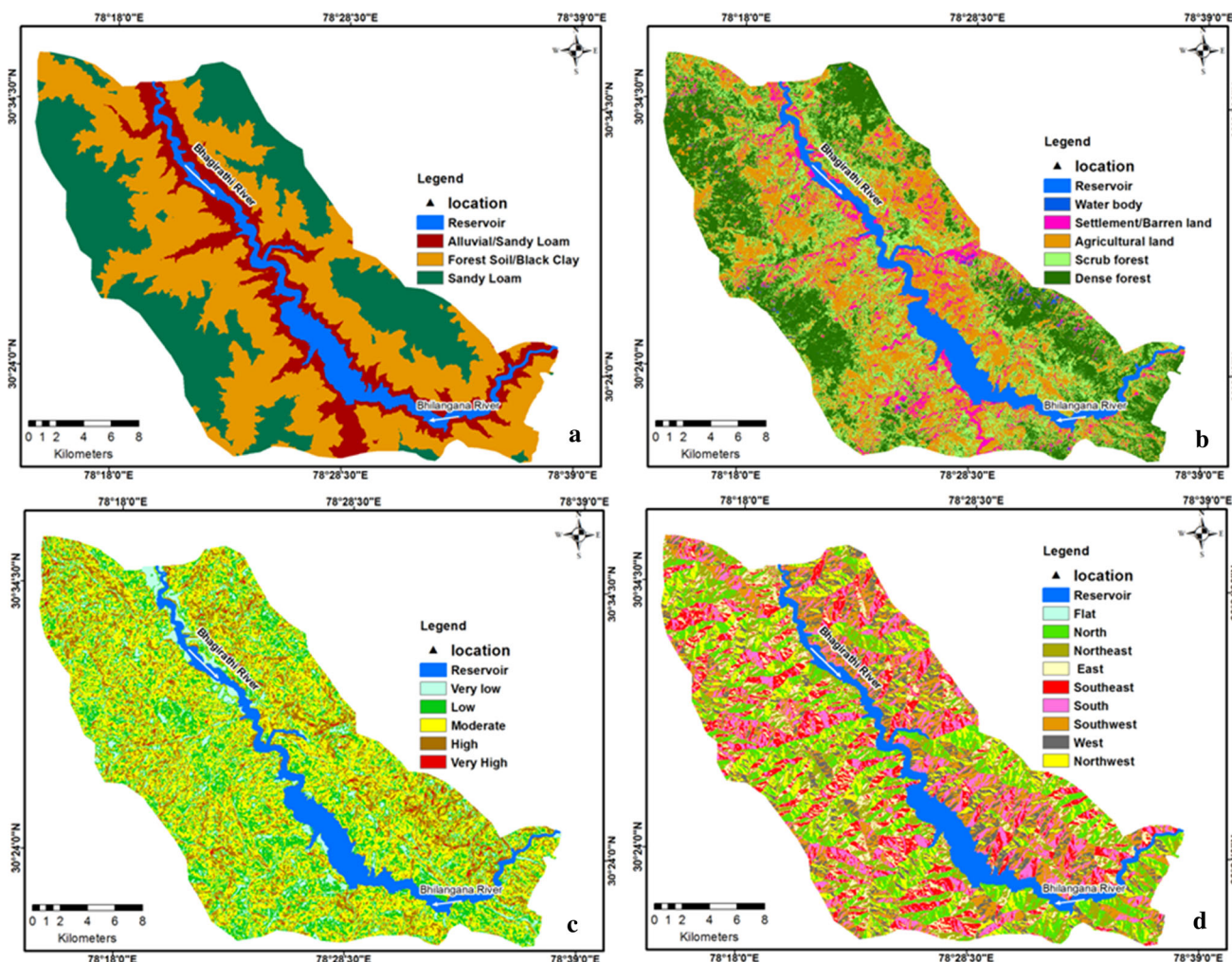


Figure 4. Maps showing landslide causative factors used in LSM preparation: (a) soil covers map, (b) land use/land cover map, (c) topographic slope (angle) map and (d) topographic aspect map.

3.5 Aspect

The topographic aspect often influences landslide susceptibility. The slope aspect governs the concentration of sunlight on slopes, which is connected to temperature and the interrelated climatic condition. In this Lesser Himalayan area, the effect of the topographic aspect can be noticed in terms of forested, wet and warm south-facing slopes, whereas largely dry and cold in north-facing slopes. Due to high precipitation, slopes having the south aspect face more number of landslides in the Himalaya. In this work, the aspect was derived from DEM and then classified into nine classes (figure 4d).

3.6 Relative relief

Relative relief is the contrast between the highest and the lowest elevation within a facet or area

(Anbalagan 1992). In this study, DEM was used to extract relative relief and was found in a range of 0–367 m. The range of relative relief was grouped into five classes, namely, very low relief (0–30 m), low relief (30–60 m), moderate relief (60–100 m), high relief (100–150 m) and very high relief (>150 m) for the LSM (figure 5a). Field inspections have indicated that areas of high relative relief are more vulnerable to landslide compared to those of low relative relief.

3.7 Lineaments

Geological structures such as faults, folds, fractures, shear zones, ridges and spurs are widely distributed in the study area. The area is represented by three regional geological structures which include two synclines and a thrust fault named NAT (figure 2). Depressions of variable dimensions were observed all through the axial zone of

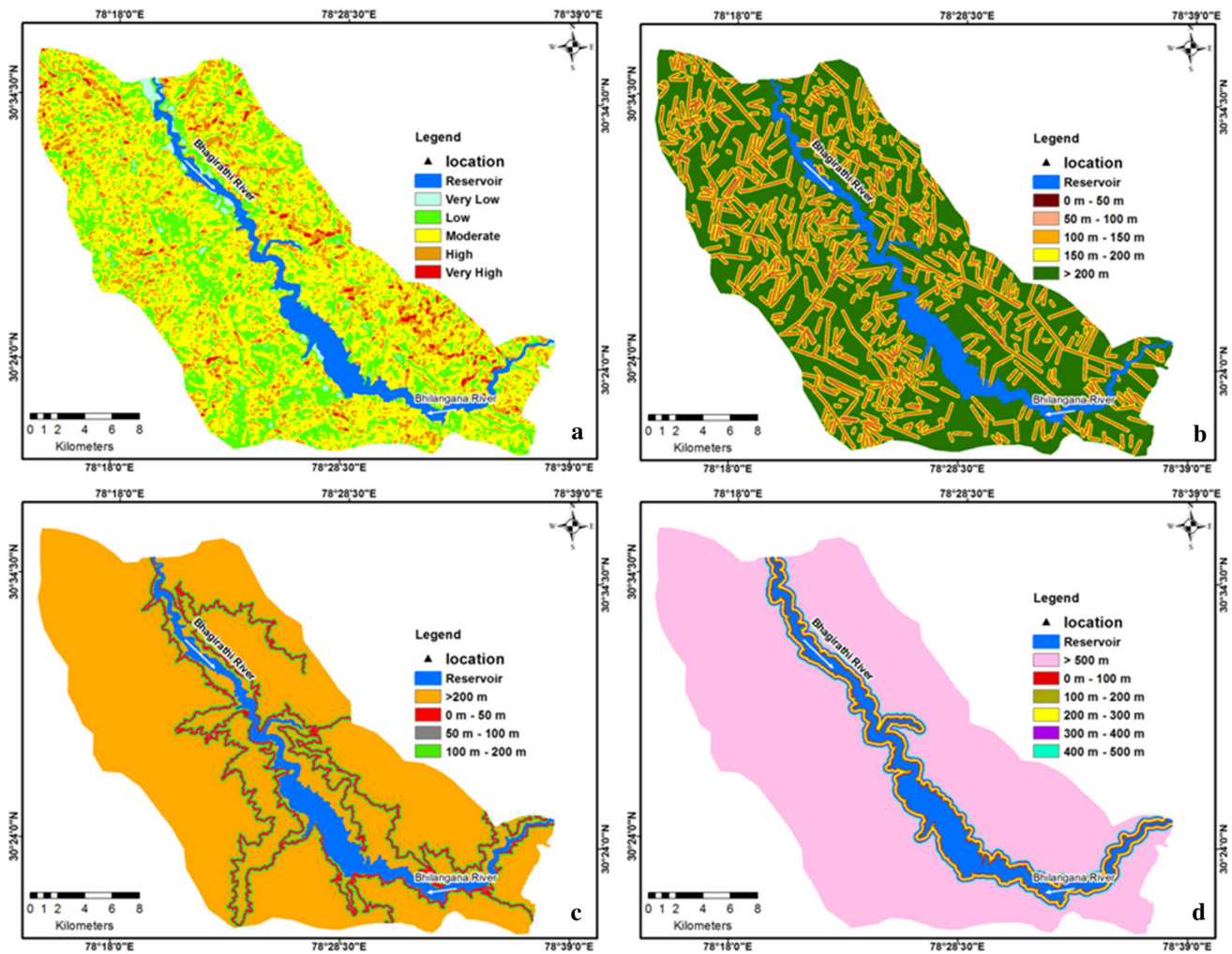


Figure 5. (a) Topographic relative relief map, (b) lineament buffer (or distance to lineament) map, (c) road buffer map and (d) reservoir buffer map.

synclines. NAT crosses through the eastern and the north-eastern side of the area and crosses the reservoir at Chham. Where NAT crosses the reservoir, it forms visible scrap faces on the left bank adjoining the river course. Linear structural discontinuities were captured in the form of photo-lineaments with the help of high resolution satellite images and DEM (figure 5b). It is a common knowledge that landslides are more likely to occur near lineaments. A lineament buffer zone (or distance to lineament) map covering 50, 100, 150 and 200 m distances was prepared as per the distribution of landslides recorded in proximity to the lineaments. Landslide density was found to be higher around the close proximity of lineaments.

3.8 Distance to drainage

Drainage of the area was delineated from the DEM. The area has a high drainage density and high

stream order (up to fifth order – Bhagirathi). The rugged topography of the area supports a deeply incised drainage system. Landslides are often found to be associated with drainage (Kumar and Anbalagan 2016). In the mountainous terrain, rivers constantly erode their banks and make sharply dipping slopes which often become the site of progressive landslide. A large number of such landslides were seen in the field. In compliance with the field evidence, the distance to the drainage (drainage buffer – 50, 100, 150 and 200 m) was prepared.

3.9 Distance to the road

A large number of landslides were recorded on the untreated cut-slopes, which occurred during the construction of the road. Most of the cut-slopes are dipping towards the road at steep angles. Throughout the rainy season, cut-slopes become highly

vulnerable to landslides. Landslides on the road cut-slopes were seen advancing at the upper levels of the main slope body. The distance to the road (road buffer – 50, 100 and 200 m) layer was generated as per the field observation (figure 5c).

3.10 Distance to the reservoir rim

During the reservoir drawdown (water level recedes >50 m), slopes saturate with moisture. The saturated portion of the slopes has been failing at a number of places. This type of reservoir-induced failures tends to advance at the upper reaches. The distribution of reservoir-induced landslides was recorded at the time of field observation, and accordingly, a buffer zone of reservoirs (100, 200, 300, 400 and 500 m) was prepared (figure 5d).

4. Methodology

WofE is a data-oriented method, which is primarily a Bayesian method in the log-linear structure using prior and posterior probability (P). The WofE technique is employed when necessary data are available to approximate the relative significance of evidential parameters using statistics (Bonham-Carter 1994; Pradhan *et al.* 2010). The WofE method works on the principles of conditional probability and it leads to the determination of the weight of a predictive pattern, B (factor/class) given the known occurrence D (landslide). Weights of the predictive pattern are synthesised on the basis of the favourability of locating an event given the presence and absence of the evidential theme (Pradhan *et al.* 2010). Bonham-Carter *et al.* (1989) synthesised the mathematical formulation to deduce the posterior probability of occurrence D , given the predictive pattern/factor B in terms of an odds-type formulation where the odds, O , are defined as $O = P/(1 - P)$:

$$O \{D|B\} = O \{D\} \frac{P \{B|D\}}{P \{B|\bar{D}\}}, \quad (1)$$

$$O \{D|\bar{B}\} = O \{D\} \frac{P \{\bar{B}|D\}}{P \{\bar{B}|\bar{D}\}}. \quad (2)$$

Weights for each landslide predictive pattern are computed on the basis of the presence or the absence of landslides within it:

$$W^+ = \log_e \frac{P \{B|D\}}{P \{B|\bar{D}\}}, \quad (3)$$

$$W^- = \log_e \frac{P \{\bar{B}|D\}}{P \{\bar{B}|\bar{D}\}}, \quad (4)$$

where P denotes the probability, W^+ and W^- are the weights for the presence or absence of landslides within a factor class, B refers to the presence of landslide predictive pattern, \bar{B} refers to the absence of predictive pattern, D denotes the landslide occurrence and \bar{D} denotes the landslide non-occurrence. The weights can be computed by cross-tabulating the observed landslide map with the landslide conditioning factor map using the equation below:

$$W^+ = \log_e \frac{\{N(B \cap D) / N(D)\}}{\{N(B \cap \bar{D}) / N(\bar{D})\}}, \quad (5)$$

$$W^- = \log_e \frac{\{N(\bar{B} \cap D) / N(D)\}}{\{N(\bar{B} \cap \bar{D}) / N(\bar{D})\}}, \quad (6)$$

where $N\{A\}$ represents the number of pixels on the map when $\{A\}$ occurs. For n number of predictive patterns ($B_i, i = 1, 2, \dots, n$), the posterior odd probability can be calculated using the formula given below, assuming that the predictive patterns are conditionally independent:

$$\log_e O \{D|B_1^s \cap B_2^s \dots B_n^s\} = \sum_{i=1}^n W_i^s + \log_e O \{D\}, \quad (7)$$

where s is positive or negative corresponding to whether the predictive pattern is present or absent, respectively. Posterior odds can be converted to posterior probabilities, based on the relation $P = (O/1 + O)$ (Lee *et al.* 2002). The statistical significance of the weights can be tested on the basis of their variances (S^2), which can be estimated roughly as (Bonham-Carter 1994; Kayastha *et al.* 2012)

$$S^2 (W^+) = \frac{1}{N(B \cap D)} + \frac{1}{N(B \cap \bar{D})}, \quad (8)$$

$$S^2 (W^-) = \frac{1}{N(\bar{B} \cap D)} + \frac{1}{N(\bar{B} \cap \bar{D})}. \quad (9)$$

A positive weight (W^+) reflects that the predictive pattern is present at the landslide locations and the magnitude of this weight is the manifestation of the positive correlation between the presence of the predictive pattern and the landslides. A negative weight (W^-) refers to the absence of

Table 3. Computed weights (W^+ , W^-) contrast (C), standard deviation (SW^- , SW^+ , SC) and studentised contrast (c/s) for classes of various data layers.

Class	Area (km ²)	Area (%)	L (%)	W^+	SW^+	W^-	SW^-	C	SC	c/s
Lithology										
Blaini formation	48.30	8.694	0.00	0.00	0.00	0.00	0.00	0.00	0.00	0.00
Nagthat formation	121.07	21.793	20.15	-0.08	0.19	0.02	0.10	-0.10	0.22	-0.46
Chandpur formation	234	41.76	55.97	0.46	0.12	-0.38	0.13	0.84	0.17	4.82
Berinag formation	76.80	13.826	14.18	0.03	0.23	0.00	0.09	0.03	0.25	0.12
Rautgara formation	41.57	7.490	2.99	-0.92	0.50	0.05	0.09	-0.97	0.51	-1.91
Deoban formation	34.69	5.235	2.99	-0.74	0.50	0.03	0.09	-0.77	0.51	-1.52
Mandhali formation	3.91	1.202	0.00	0.00	0.00	0.00	0.00	0.00	0.00	0.00
Soil cover										
Alluvial/sandy loam	84.092	15.003	55.97	2.354	0.216	-0.766	0.137	3.120	0.256	12.205
Forest soil/black clay	283.808	50.634	35.82	-0.413	0.155	0.336	0.124	-0.749	0.199	-3.766
Sandy loam	192.603	34.363	8.21	-1.597	0.309	0.434	0.105	-2.032	0.326	-6.229
LULC										
Water body	6.570	1.182	1.492	0.298	0.813	-0.004	0.097	0.302	0.819	0.369
Settlement/barren land	37.142	6.683	17.164	1.413	0.294	-0.146	0.104	1.559	0.312	5.004
Agricultural land	123.805	22.276	28.358	0.309	0.187	-0.100	0.113	0.409	0.218	1.875
Scrub/open forest	209.616	37.715	37.313	-0.013	0.157	0.008	0.122	-0.021	1.199	-0.107
Dense forest/vegetation	178.648	32.144	15.671	-0.834	0.229	0.277	0.108	-1.111	0.253	-4.385
Slope angle										
0-8°	27.684	4.939	3.73	-0.337	0.484	0.016	0.098	-0.352	0.493	-0.714
8-18°	136.630	24.374	7.46	-1.336	0.326	0.256	0.103	-1.592	0.342	-4.658
18-30°	288.293	51.429	47.01	-0.110	0.139	0.109	0.133	-0.219	0.192	-1.136
30-42°	104.875	18.709	41.04	1.117	0.177	-0.384	0.121	1.502	0.215	7.000
>42°	3.081	0.550	0.75	0.395	1.162	-0.002	0.096	0.397	1.166	0.340
Slope aspect										
North	18.859	3.366	3.73	0.129	0.504	-0.005	0.098	0.134	0.513	0.261
North-east	98.793	17.633	8.96	-0.788	0.304	0.125	0.102	-0.913	0.321	-2.849
East	36.655	6.542	5.97	-0.112	0.389	0.008	0.099	-0.120	0.402	-0.298
South-east	87.373	15.594	25.37	0.647	0.207	-0.150	0.110	0.798	0.234	3.409
South	83.952	14.984	27.61	0.834	0.204	-0.195	0.111	1.029	0.233	4.426
South-west	81.435	14.534	9.70	-0.480	0.297	0.069	0.102	-0.548	0.314	-1.747
West	37.120	6.625	1.49	-1.659	0.723	0.067	0.097	-1.725	0.729	-2.365
North-west	75.934	13.553	8.96	-0.492	0.309	0.065	0.101	-0.556	0.325	-1.711
North	40.123	7.161	8.21	0.172	0.341	-0.014	0.100	0.186	0.356	0.523
Relative relief										
Very low	8.405	1.499	1.49	-0.006	0.786	0.000	0.097	-0.006	0.792	-0.007
Low	145.779	26.005	8.21	-1.303	0.311	0.274	0.103	-1.577	0.328	-4.812
Moderate	316.705	56.496	58.96	0.053	0.126	-0.072	0.149	0.124	0.195	0.638
High	81.805	14.593	29.10	0.958	0.204	-0.226	0.112	1.184	0.232	5.097
Very high	7.888	1.407	2.24	0.615	0.692	-0.011	0.097	0.625	0.699	0.895
Lineament buffer (distance to lineament)										
0-50 m	36.103	6.441	5.97	-0.093	0.390	0.006	0.099	-0.099	0.402	-0.247
50-100 m	38.707	6.906	2.24	-1.275	0.596	0.061	0.098	-1.336	0.604	-2.211
100-150 m	79.273	14.143	5.97	-0.991	0.369	0.114	0.100	-1.104	0.382	-2.890
150-200 m	73.983	13.199	8.21	-0.561	0.321	0.070	0.101	-0.630	0.337	-1.872
>200 m	332.439	59.311	77.61	0.345	0.113	-0.699	0.193	1.043	0.224	4.662
Drainage buffer										
0-50 m	14.983	2.684	11.19	0.77	0.26	-0.69	0.082	1.33	0.28	4.76
50-100 m	15.537	2.783	11.19	1.26	0.26	-0.067	0.082	1.29	0.28	4.62
100-150 m	31.330	5.613	21.64	1.23	0.19	-0.137	0.086	1.3	0.21	6.26
150-200 m	31.722	5.683	14.93	1.18	0.23	-0.071	0.083	0.84	0.24	3.48
>200 m	464.636	83.237	64.93	-0.47	0.108	1.08	0.11	-1.55	0.158	-9.81

Table 3. (Continued.)

Class	Area (km ²)	Area (%)	L (%)	W ⁺	SW ⁺	W ⁻	SW ⁻	C	SC	c/s
Road buffer										
0–50 m	32.301	5.785	38.81	1.904	0.139	-0.432	0.110	2.336	0.177	13.172
50–100 m	27.960	5.008	5.22	0.042	0.378	-0.002	0.089	0.045	0.388	0.115
100–200 m	46.575	8.342	5.97	-0.335	0.354	0.026	0.089	-0.360	0.365	-0.988
>200 m	451.489	80.865	50.00	-0.481	0.122	0.961	0.122	-1.442	0.173	-8.343
Reservoir buffer										
0–100 m	13.776	2.458	14.93	1.805	0.224	-0.137	0.094	1.942	0.243	8.005
100–200 m	12.904	2.302	26.87	2.459	0.167	-0.290	0.101	2.749	0.195	14.092
200–300 m	12.256	2.187	8.21	1.323	0.302	-0.064	0.090	1.387	0.315	4.406
300–400 m	11.620	2.073	0.75	-1.022	1.000	0.014	0.087	-1.035	1.004	-1.031
400–500 m	11.141	1.988	3.73	0.630	0.447	-0.018	0.088	0.648	0.456	1.421
>500 m	498.807	88.993	45.52	-0.670	0.128	1.600	0.117	-2.270	0.174	-3.085

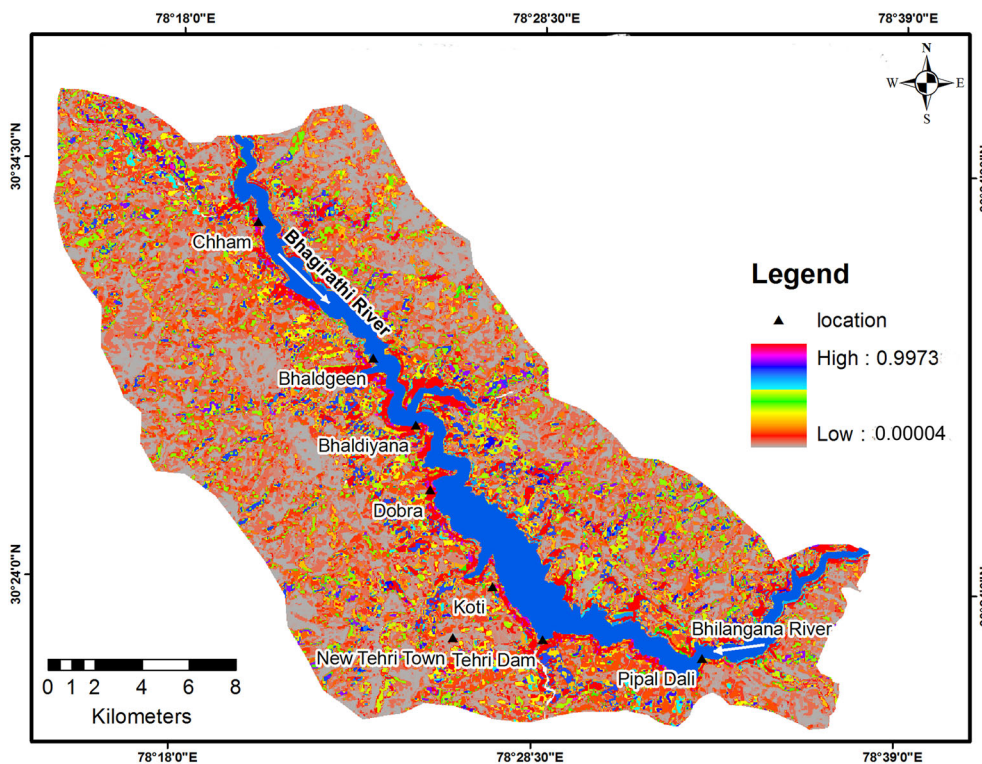


Figure 6. Map of posterior landslide probability computed using the WofE method.

the predictive pattern and shows the degree of negative correlation (Dahal et al. 2008). The contrast (C) between W^+ and W^- is

$$C = W^+ - W^-, \tag{10}$$

reflects the spatial correlation between the predictive pattern and the landslides. For a spatial association, the value of C is positive, and for disassociation, the contrast takes a negative value.

5. Analytical results and discussion

The initial steps involved the generation of a training data set, in which a total of 134 (out of 195) landslide occasions were randomly chosen for the training and the rest of the 61 landslides were left for validation. To carry out WofE in the present study, the Arc SDM extension of the ArcGIS 9.3 software was used. The extension has several tools to compute the posterior probability map along

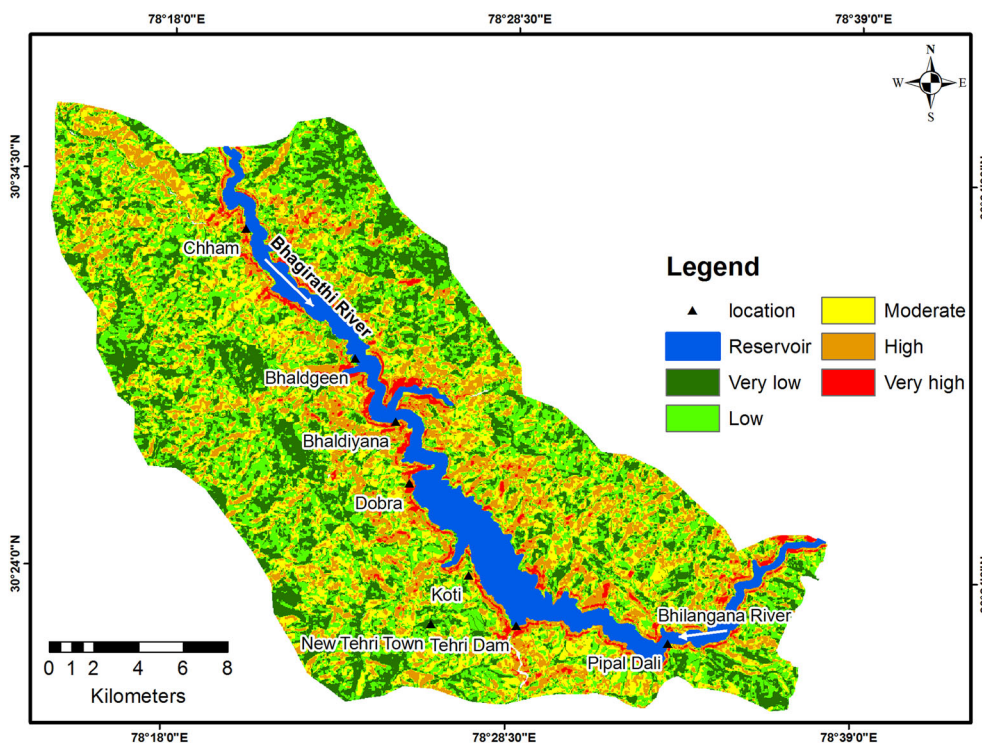


Figure 7. Landslide susceptibility map of the Tehri reservoir rim area.

with a Grand WofE tool which computes W^+ , W^- and the posterior probability map, etc., in a single step. All 10 factor maps were subjected to grand WofE tool of the Arc SDM, which resulted in a grand table (table 3) containing W^+ , W^- , C , $S^2(W^+)$, $S^2(W^-)$, $S^2(C)$ and $C/S(C)$ information of each of the factor class using equations (5, 6 and 8–10). It also resulted in a posterior probability map containing the information of probability (in a range of 0–1) of landslide occurrence on a cell-by-cell basis by using equation (7) (figure 6). In general practice, some degree of conditional dependence amongst the predictor maps always exists (Bonham-Carter 1994; Mihalasky 1999; Porwal *et al.* 2003), which results in the artificial inflation or deflation of the posterior probability. Henceforth, the posterior probability map should be considered largely as a relative ranking of landslide propensity (on a cell-by-cell basis) rather than the corresponding posterior probability values having any direct meaning (Porwal *et al.* 2003; Fabbri and Chung 2008).

6. Landslide susceptibility mapping

As mentioned in the previous section, the posterior probabilities should not be considered in

Table 4. Threshold values used for classifying posterior probability map into relative susceptibility classes and the resulting area occupied by those classes.

LSM class	Threshold value	Area occupied (km ²)
Very low	0.014	121.55
Low	0.06	164.4
Moderate	0.19	141.2
High	0.52	106.6
Very high	0.997	16.25

absolute terms, but as a relative term of landslide favourability, which can be depicted by the relative landslide susceptible map instead of using the actual posterior probability values. Arc-SDM’s GWofE outputs a continuous raster, which represents landslide probability in a continuous scale from 0 (minimum) to 1 (maximum). In the present case, a minimum probability value of 0.00004 and a maximum of 0.9973 were observed. Jenk’s natural break method (ESRI F 2012) was used to classify the posterior probability map into relative landslide susceptibility classes (figure 7) as indicated in table 4. This table also refers to the area occupied under different LSM classes.

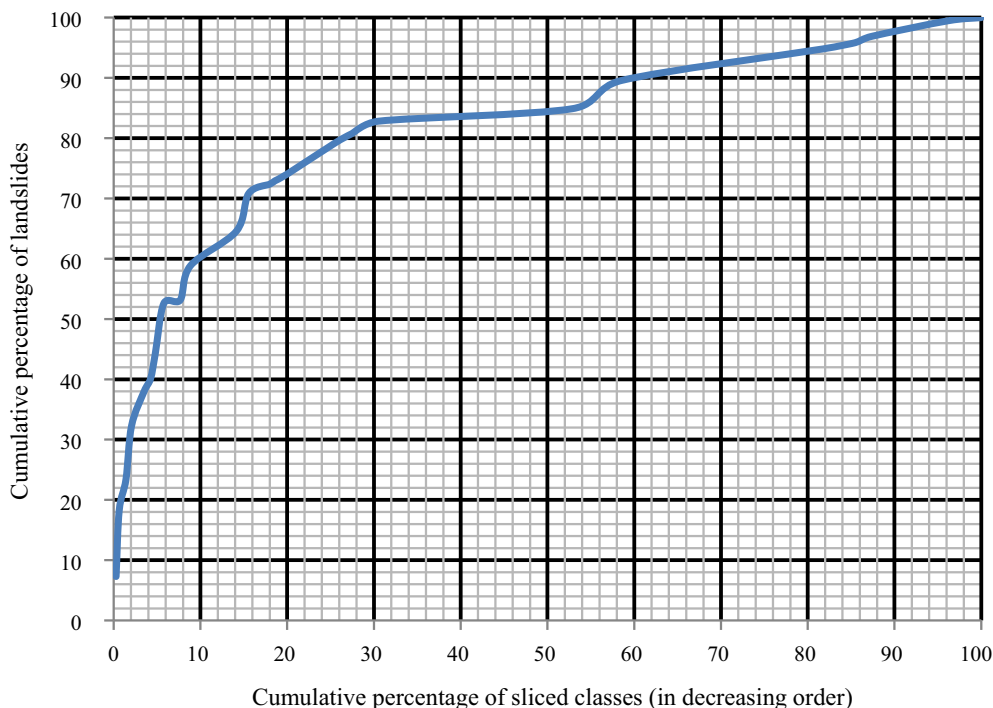


Figure 8. Curve showing the cumulative percentage of landslide occurrences *vs.* cumulative percentage of the decreasing landslide susceptibility index value.

7. Conditional independence (CI) test

The WofE method considers the CI between the landslide factors, in which each factor induces ‘independent’ evidence of favourability. [Agterberg and Cheng \(2002\)](#) arrived at the conclusion that for all conditionally independent factors, the numbers of observed and predicted occurrence will be equal. However, when working with data containing a wide range of information, CI is constantly disobeyed to some degree ([Bonham-Carter 1994](#); [Porwal et al. 2003](#)). In this work, the omnibus test, also known as the ‘Agterberg–Cheng test’ was exercised for the delineation of CI between the landslide factors and factor classes. The omnibus test reveals whether the number of predicted occurrences (T) and the number of observed occurrence ($T - n$) are ‘significantly >0 ’. This is a one-tailed test of the null hypothesis that $T - n = 0$ ([Agterberg and Cheng 2002](#)). The test statistic is $(T - n)/\sigma T$. Probability values $>95\%$ or 99% show that the hypothesis of CI should be rejected, but any value $>50\%$ points out that some degree of conditional dependence happens ([Agterberg and Cheng 2002](#)). The test has been suggested as providing the most reliable approach for testing for CI ([Thiart et al. 2006](#)). CI tests within the factors and factor classes were carried out in the Arc SDM extension of

the ArcGIS 9.3 software. More than 70% of the combinations (factors/classes: between them tests were carried out) gave a fair degree of CI, while the rest of the combinations resulted in varying degrees of dependence.

8. Validation

In this work, the success rate/cumulative percentage curve method was applied to accomplish the accuracy assessment of LSM. The curve was formed by plotting the cumulative per cent of the susceptibility index (posterior probability) in descending order on the X-axis and the cumulative percentage of landslide on the Y-axis. The curve was generated using the 61 landslide incidences spared for the accuracy assessment. The posterior probability map was sliced into 25 classes according to the natural break thresholds and cross-tabulated with the landslides present in each sliced class in descending order of the probability classes. Cumulative percentage of the area of sliced classes and landslide present in those were calculated to generate the cumulative percentage curve (figure 8). The curve shows that 60% landslide falls under the initial 10% of high probability class and more than 75% landslide falls under the

initial 20% of high probability classes. This clearly indicates the prediction capability of the WofE-based LSM method. The value of the area under curve (AUC) was estimated through the simple trapezium method, which gave a value of 0.83. AUC value of 0.83 can be interrelated as 83% of accuracy in identifying landslide probable zones.

9. Conclusions

Landslides have become a frequent phenomenon in the Tehri reservoir rim area. Reservoir water fluctuation (mainly between the monsoon and lean seasons) and construction activities such as roads, modern buildings, etc., in the rim area have added further stress. The LSM of slopes bounding the reservoir can provide important inputs in long-term planning that include reservoir operation, reservoir sedimentation, land-use, etc. A comprehensive landslide inventory is required to carry out LSM. For this study, field-based observation and a high resolution satellite image were used to generate the landslide inventory.

The WofE technique was applied to understand the relationship between factor attributes and landslides. It has given positive and negative correlation values in numerical form. Furthermore, this technique was applied to generate a posterior probability map in which each mapping unit contains a landslide probability value. The results show the robustness of the WofE technique in mapping landslide susceptible areas with uniform landslide distribution. Planners can quickly identify susceptible areas if a detailed landslide inventory is available. Based on positive and negative contract (C) values, important factors responsible for landslide can be identified.

High positive C values are observed in rocks belonging to the Chandpur formation, high slope category ($30\text{--}44^\circ$), alluvial soil, settlement/barren land, south facing aspect, high relative relief (150–200 m), very high proximity to drainage (0–50 m), very high proximity to road (0–50 m) and very high proximity to the reservoir (0–100 m). Factors which are found to have no influence (high negative contract values) are the rocks belonging to the Blaini and Rautgara formations, forest soil, low slope areas ($8\text{--}18^\circ$), north-east and north-west slope aspects, low relative relief areas (30–60 m), low proximity to drainage (>200 m), low proximity to roads (>200 m) and low proximity to the reservoir (>500 m).

The WofE technique has given reasonable (83%) accuracy in mapping susceptible areas. Accuracy was assessed by applying the AUC technique. The final map establishes that approximately 50% of the reservoir rim area falls in a moderate to very high susceptible zone. This is very important for the planners since the Tehri dam and the reservoir are a great asset to this country; hence, proper reservoir rim area planning is required for the long-term functioning.

Acknowledgements

The authors acknowledge THDCL, Rishikesh, for giving ancillary help throughout this work. They offer their sincere gratitude to the Department of Earth Sciences, IIT Roorkee, for providing laboratory and software facility for carrying out this work. They also acknowledge Punjab Engineering College, Chandigarh, for allowing them to complete the paper.

References

- Agterberg F P and Cheng Q 2002 Conditional independence test for weights of evidence modelling; *Nat. Resour. Res.* **11** 249–255.
- Akgun A and Erkan O 2016 Landslide susceptibility mapping by geographical information system-based multivariate statistical and deterministic models: In an artificial reservoir area at Northern Turkey; *Arab. J. Geosci.* **9** 1–15.
- Akgun A, Dag S and Bulut F 2008 Landslide susceptibility mapping for a landslide-prone area (Findikli, NE of Turkey) by likelihood frequency ratio and weighted linear combination models; *Environ. Geol.* **54**(6) 1127–1143.
- Anbalagan R 1992 Landslide hazard evaluation and zonation mapping in mountainous terrain; *Eng. Geol.* **32** 269–277.
- Anbalagan R, Kumar R, Lakshmanan K, Parida S and Neethu S 2015 Landslide hazard zonation mapping using frequency ratio and fuzzy logic approach, a case study of Lachung Valley, Sikkim; *Geoenviron. Disasters* **2**(1) 1–17, <https://doi.org/10.1186/s40677-014-0009-y>.
- Arora M K, Das Gupta A S and Gupta R P 2004 An artificial neural network approach for landslide hazard zonation in the Bhagirathi (Ganga) Valley, Himalayas; *Int. J. Rem. Sens.* **25** 559–572.
- Bonham-Carter G F 1994 *Geographic information system for geoscientists: Modelling with GIS*; Pergamon, Oxford, 398p.
- Bonham-Carter G F, Agterberg F P and Wright D F 1989 Weights of evidence modelling: A new approach to mapping mineral potential; In: *Statistical applications in the earth sciences* (eds) Agterberg F P and Bonham-Carter G F, *Geol. Survey Canada Paper* **89**(9) 171–183.
- Chakraborty D and Anbalagan R 2008 Landslide hazard evaluation of road cut slopes along Uttarkashi–Bhatwari

- road, Uttarakhand Himalaya; *J. Geol. Soc. India* **71** 115–124.
- Ciurleo M, Cascini L and Calvello M 2017 A comparison of statistical and deterministic methods for shallow landslide susceptibility zoning in clayey soils; *Eng. Geol.* **223** 71–81.
- Dahal R K, Hasegawa S, Nonomura S, Yamanaka M, Masuda T and Nishino K 2008 GIS-based weights-of-evidence modelling of rainfall-induced landslides in small catchments for landslide susceptibility mapping; *Environ. Geol.* **54**(2) 314–324.
- Das I, Stein A and Dadhwal V K 2012 Landslide susceptibility mapping along road corridors in the Indian Himalayas using Bayesian logistic regression models; *Geomorphology* **179** 116–125.
- Dobhal D P, Gupta A K, Mehta M and Khandelwal D D 2013 Kedarnath disaster: Facts and plausible causes; *Curr. Sci.* **105** 171–174.
- ESRI F 2012 What is the Jenks optimization method? <http://support.esri.com/en/knowledgebase/techarticles/detail/26442>.
- Fabbri A G and Chung C J 2008 On blind tests and spatial prediction models; *Nat. Resour. Res.* **17**(2) 107–118.
- Fritz H M, Phillips D A, Okayasu A, Shimozono T, Liu H, Fahad M, Skanavis V, Synolakis C E and Takahashi T 2012 The 2011 Japan tsunami current velocity measurements from survivor videos at Kesennuma Bay using LiDAR; *Geophys. Res. Lett.* **39** L00G23, <https://doi.org/10.1029/2011GL050686>.
- Ghosh S, Van Westen C J, Carranza E J M, Ghoshal T B, Sarkar N K and Surendranath M 2009 A quantitative approach for improving the BIS (Indian) method of medium-scale landslide susceptibility; *J. Geol. Soc. India* **74**(5) 625–638.
- Gupta P and Anbalagan R 1997 Landslide hazard zonation (LHZ) and mapping to assess slope stability of parts of the proposed Tehri dam reservoir, India; *Quart. J. Eng. Geol.* **30** 27–36.
- Gupta R P 2018 *Remote sensing geology*; Springer, Berlin, Heidelberg, <https://doi.org/10.1007/978-3-662-55876-8>.
- Gupta R P, Kanungo D P, Arora M K and Sarkar S 2008 Approaches for comparative evaluation of raster GIS-based landslide susceptibility zonation maps; *Int. J. Appl. Earth Obs. Geoinf.* **10** 330–341.
- Guzzetti F, Carrara A, Cardinali M and Reichenbach P 1999 Landslide hazard evaluation: A review of current techniques and their application in a multi-scale study, central Italy; *Geomorphology* **31** 181–216.
- Hong H, Liu J, Tien Bui D, Pradhan B, Acharya T D, Pham B T, Zhu A X, Chen W and Bin Ahmad B 2018 Landslide susceptibility mapping using J48 decision tree with AdaBoost, bagging and rotation forest ensembles in the Guangchang area (China); *Catena* **163** 399–413.
- Kalantar B, Pradhan B, Naghibi S A, Motevalli A and Mansor S 2018 Assessment of the effects of training data selection on the landslide susceptibility mapping: A comparison between support vector machine (SVM), logistic regression (LR) and artificial neural networks (ANN); *Geomat. Nat. Haz. Risk* **9**(1) 49–69.
- Kannan M, Saranathan E and Anbalagan R 2013 Landslide vulnerability mapping using frequency ratio model: A geospatial approach in Bodi–Bodimettu Ghat section, Theni district, Tamil Nadu, India; *Arab. J. Geosci.* **6**(8) 2901–2913.
- Kanungo D P, Arora M K, Sarkar S and Gupta R P 2006 A comparative study of conventional, ANN black box, fuzzy and combined neural and fuzzy weighting procedures for landslide susceptibility Zonation in Darjeeling Himalayas; *Eng. Geol.* **85** 347–366.
- Kayastha P, Dhital M R and De Smedt F 2012 Landslide susceptibility mapping using weight of evidence in the Tinau watershed, Nepal; *Nat. Hazards* **63**(2) 479–498.
- Kirschbaum D, Adler R, Hong Y, Hill S and Lerner-Lam A 2010 A global landslide catalog for hazard application: Method, result, and limitations; *Nat. Hazards* **52** 561–575.
- Kouli M, Loupasakis C, Soupios P, Rozos D and Vallianatos F 2013 Comparing multi-criteria methods for landslide susceptibility mapping in Chania Prefecture, Crete Island, Greece; *Nat. Hazards Earth Syst. Sci. Discuss.* **1** 73–109.
- Kumar R and Anbalagan R 2015 Landslide susceptibility zonation in part of Tehri reservoir region using frequency ratio, fuzzy logic and GIS; *J. Earth Syst. Sci.* **124**(2) 431–448.
- Kumar R and Anbalagan R 2016 Landslide susceptibility mapping using analytical hierarchy process (AHP) in Tehri reservoir rim region, Uttarakhand; *J. Geol. Soc. India* **87**(3) 271–286.
- Kumar D, Thakur M, Dubey C S and Shukla D P 2017 Landslide susceptibility mapping & prediction using support vector machine for Mandakini River Basin, Garhwal Himalaya, India; *Geomorphology* **295** 15–125.
- Kundu S, Saha A K, Sharma D C and Pant C C 2013 Remote sensing and GIS based landslide susceptibility assessment using binary logistic regression model: A case study in the ganeshganga watershed, Himalayas; *J. Indian Soc. Rem. Sens.* **41**(3) 697–709.
- Lee S, Choi J and Min K 2002 Landslide susceptibility analysis and verification using the Bayesian probability model; *Environ. Geol.* **43** 120–131.
- Mathew J, Jha V K and Rawat G S 2007 Weights of evidence modelling for landslide hazard zonation mapping in part of Bhagirathi valley, Uttarakhand; *Curr. Sci.* **92**(5) 628–638.
- Mihalasky M J 1999 Mineral potential modelling of gold and silver mineralization in the Nevada Great Basin: A GIS-based analysis using weights of evidence; Unpublished Doctoral Dissertation, Univ. Ottawa.
- Nandi A and Shakoor A 2009 A GIS-based landslide susceptibility evaluation using bivariate and multivariate statistical analyses; *Eng. Geol.* **110** 11–20.
- NDMA 2009 *Management of landslides and snow avalanches*; National Disaster Management Authority (NDMA), Government of India, New Delhi, 144p.
- OFDA/CRED 2010 *EM-DAT International disaster database* -<http://www.em-dat.net>; Universite Catholique de Louvain, Brussels, Belgium.
- Pardeshi S D, Autade S E and Pardeshi S S 2013 Landslide hazard assessment: Recent trends and techniques; *Springerplus* **523**(2) 1–11.
- Porwal A, Carranza E J M and Hale M 2003 Knowledge-driven and data-driven fuzzy models for predictive mineral potential mapping; *Nat. Resour. Res.* **12** 1–25.

- Pourghasemi H R, Pradhan B and Gokceoglu C 2012 Application of fuzzy logic and analytical hierarchy process (AHP) to landslide susceptibility mapping at Haraz watershed, Iran; *Nat. Hazards* **63**(2) 965–996.
- Pradhan B 2010 Landslide susceptibility mapping of a catchment area using frequency ratio, fuzzy logic and multivariate logistic regression approaches; *J. Indian Soc. Rem. Sens.* **38**(2) 301–320.
- Pradhan B, Hyon-Joo Oh and Buchroithner M 2010 Use of remote sensing data and GIS to produce a landslide susceptibility map of a landslide prone area using a weight of evidence model; *Geomatics, Natural Hazards and Risk, Remote Sensing Science Center for Cultural Heritage*, pp. 395–402.
- Saha A K, Gupta R P, Sarkar I, Arora M K and Csaplovics E 2005 An approach for GIS-based statistical landslide susceptibility zonation with a case study in the Himalayas; *Landslides* **2** 61–69.
- Sarkar S, Roy A K and Raha P 2016 Deterministic approach for susceptibility assessment of shallow debris slide in the Darjeeling Himalayas, India; *Catena* **142** 36–46.
- Shahabi H, Hashim M and Ahmad B B 2015 Remote sensing and GIS-based landslide susceptibility mapping using frequency ratio, logistic regression, and fuzzy logic methods at the central Zab basin, Iran; *Environ. Earth Sci.* **73** 8647–8668.
- Sharma S and Mahajan A K 2018 A comparative assessment of information value, frequency ratio and analytical hierarchy process models for landslide susceptibility mapping of a Himalayan watershed, India; *Bull. Eng. Geol. Environ.*, <https://doi.org/10.1007/s10064-018-1259-9>.
- Sujatha E R, Kumaravel P and Rajamanickam G V 2014 Assessing landslide susceptibility using Bayesian probability-based weight of evidence model; *Bull. Eng. Geol. Environ.* **73**(1) 147–161.
- Thiart C, Bonham-Carter G F, Agterbreg F P, Cheng Q and Panahi A 2006 An application of the new omnibus test of conditional independence in weights-of-evidence modelling; In: *GIS for the earth sciences* (ed.) Harris J R, Vol. **44**, Geological Association of Canada, Special Publication, pp. 131–142.
- Umar Z, Pradhan B, Ahmad A, Jebur M N and Tehrany M S 2014 Earthquake-induced landslide susceptibility mapping using an integrated ensemble frequency ratio and logistic regression models in West Sumatera Province, Indonesia; *Catena* **118** 124–135.
- Valdiya K S 1980 Geology of Kumaun Lesser Himalaya Interim Report 291, Wadia Institute of Himalayan Geology, Dehradun.
- Varnes D J 1984 *International association of engineering geology commission on landslides and other mass movements on slopes: Landslide hazard zonation: A review of principles and practice*; UNESCO, Paris, 63p.
- Watershed Management Directorate, Dehradun (WMDD) 2009 Report on Uttarakhand State perspective and strategic planning 2009–2027. <http://wmduk.gov.in/Perspective.Plan.2009-2027.pdf>.
- Yan F, Zhang Q, Ye S and Ren B 2019 A novel hybrid approach for landslide susceptibility mapping integrating analytical hierarchy process and normalized frequency ratio methods with the cloud model; *Geomorphology* **327** 170–187.
- Yao X, Tham L G and Dai F C 2008 Landslide susceptibility mapping based on support vector machine: A case study on natural slopes of Hong Kong, China; *Geomorphology* **101**(4) 572–582.
- Yilmaz I 2010 Comparison of landslide susceptibility mapping methodologies for Koyulhisar, Turkey: Conditional probability, logistic regression, artificial neural networks, and support vector machine; *Environ. Earth Sci.* **61** 821–836.

Corresponding editor: ARKOPROVO BISWAS